Determination of the mechanical properties of polymeric microneedles by micromanipulation

Du, Guangsheng ; Zhang, Zhihua; He, Penghui ; Zhang, Zhibing; Sun, Xun

DOI:
10.1016/j.jmbbm.2021.104384

Document Version
Peer reviewed version

Citation for published version (Harvard):
Du, G, Zhang, Z, He, P, Zhang, Z & Sun, X 2021, 'Determination of the mechanical properties of polymeric microneedles by micromanipulation ', *Journal of the Mechanical Behavior of Biomedical Materials*, vol. 117, 104384. https://doi.org/10.1016/j.jmbbm.2021.104384

Determination of the mechanical properties of polymeric microneedles by micromanipulation

Guangsheng Du[1], Zhihua Zhang[2], Penghui He[1], Zhibing Zhang[2*] and Xun Sun[1*]

[1] West China School of Pharmacy, Sichuan University, Chengdu, 610041, China

[2] School of Chemical Engineering, University of Birmingham, Edgbaston, Birmingham B15 2TT, UK

*Corresponding author

E-mail address: sunxun@scu.edu.cn; Z.Zhang@bham.ac.uk

Abstract:

Precise characterization of the mechanical properties of polymeric microneedles is crucial for their successful penetration into skin and delivery of the loaded active ingredients. However, most available strategies for this purpose are based on compression of the whole patch, which only provide the average rupture force of the needles and can not give information on the variations across individual microneedles in the patch. In this study, we determined the mechanical strength of individual microneedles of two types of hyaluronic acid microneedles with or without loaded model drugs using a micromanipulation technique. The applied force as a function of displacement of the microneedles was recorded, which was used to determine the rupture displacement, rupture force, and then to derive and calculate normal stress-deformation curve, rupture stress and Young's modulus of individual microneedles. The obtained data suggest that the molecular weight of the polymer and the loading of drug into the microneedles can significantly affect the rupture behavior and mechanical properties of the microneedles, which provides a foundation for preparing sufficiently strong microneedles for controlled drug delivery.

Keywords: Mechanical properties, Polymeric microneedles, Micromanipulation, Rupture force, Normal stress

1. Introduction

Polymeric microneedles have been widely investigated for drug delivery, medical diagnosis and health monitoring [1-3]. They can pierce skin barrier in a non-invasive and pain-free way as they do not touch nerves or blood capillaries inside the skin during application. As compared to solid and hollow microneedles made of glass or metal, polymeric microneedles made of dissolving or biodegradable polymers also hold advantages including resulting in no hazardous waste after administration and easiness for modulation of release properties of the loaded ingredients [4,5]. However, polymer based microneedles have a relatively weak mechanical strength, which may cause the breakage or bending of the microneedles during the insertion of skin, resulting in an insufficient penetration [6,7]. Direct and precise measurement of the mechanical properties of polymeric microneedles is necessary for ensuring their successful application especially in case of industrial mass production. Besides, emerging new types of advanced microneedles have been designed and investigated in the past decade, such as bio-responsive microneedles [8,9], core-shell structured microneedles [10,11], and hydrogel microneedles

[12]. Precise characterization of the mechanical properties of these microneedles is crucial for their possible translation as the complex composition and design could significantly affect their mechanical strength.

In many microneedle studies, the mechanical strength of microneedle patch was investigated by compressing the whole patch against a flat surface, after which the rupture force of single microneedles was calculated by dividing the total rupture force by the number of needles [7,13]. This strategy is not adequate since it can not identify the possible variations of the mechanical properties among the microneedles across the patch. The mechanical properties obtained are also limited to the rupture force of the bulk patch. In other microneedle studies, their mechanical properties were not directly measured but were instead reflected by their skin penetration efficiency. The small holes in the skin generated by microneedle penetration were normally stained and visualized for calculating the skin penetration efficiency [14,15]. However, this method gives no quantitative results for the mechanical property of microneedles. Atomic force microscopy (AFM) has also been used to measure the mechanical properties of microneedles. However, their indenting depth or force is limited to nanoscale measurement [16,17].

Micromanipulation is an experimental technique that was first developed for measurement of the bursting force of single mammalian cells [18]. This technique was then extended to analyze other biological or non-biological micro-particles, including microcapsules and microspheres [19-21]. Micro-particles can be rested on a glass slide or in a chamber and then compressed by using a cylindrical probe with a diameter larger than the micro-particles. As compared to other bulk methods for mechanical property characterization, the technique can record the force-displacement curves generated from compression of single micro-particles, which can be further used to extract important mechanical property parameters including rupture force, displacement at rupture and normal rupture stress [22,23]. The generated data can also be used to determine the intrinsic material properties of the samples, such as Young's modulus, yield stress and stress and strain at rupture by analytical or numerical modeling [19].

Herein, we investigated the mechanical properties of two types of home-made hyaluronic acid (HA) based dissolving microneedles with or without loaded model drugs of lidocaine hydrochloride and bupivacaine hydrochloride with a micromanipulation technique. Both of them are hydrophilic small-molecule drugs and used as local anesthetic of the amino amide type in clinic. The use of micromanipulation allows the precise measurement of the mechanical properties of individual microneedles. The force-displacement data were first recorded with this technique, which were used to determine the rupture displacement and rupture force, and then to derive normal rupture stress and Young's modulus of the microneedles. The influences of molecular weight of HA and the drug loading on the mechanical properties of the microneedles were investigated.

2. Method and materials

Materials

HA with a molecular weight of 10-kDa and 300-kDa were purchased from Bloomage Biotech (Jinan, China). Lidocaine hydrochloride and bupivacaine hydrochloride as model drugs were received as gifts

from West China Hospital of Sichuan University (Chengdu, China). Rhodamine B dye was purchased from Meilunbio (Dalian, China). Milli-Q water was used for the preparation of all solutions. All the other reagents used were of analytical grade.

Fabrication of HA based microneedles

Different types of fabricated quadrangular pyramid microneedles (700 μm height, 300 μm base width and 600 μm center-center spacing) in a 10 by 10 array on a back plate of 0.9 × 0.9 cm^2 are summarized in Table 1. All of the microneedles were fabricated by using a micro-molding method as previously reported [24]. Briefly, polydimethylsiloxane (PDMS) molds were first duplicated from stainless steel microneedle molds. Next, 30 μl HA solution dissolved with or without drugs was loaded into the cavities of a PDMS mold by using pressurized air to form the needles of the patch. After drying for 0.5 h in anhydrous silica gel environment, 40 μl of blank HA solution was added into the mold to form the back plate of the patch. Finally, the microneedle patches were dried for another 4 h and subsequently peeled off from the mold. The fabricated patches were stored in dry environment for further characterization. To fabricate microneedle patches for visualization by confocal microscopy, rhodamine B dye was dissolved in HA solution for the fabrication.

Table 1. Different types of microneedle (MN) patches characterized in the current study

MN type	Matrix	Abbreviation name
1	10-kDa HA	Blank HA (10-kDa) MN
2	300-kDa HA	Blank HA (300-kDa) MN
3	Bupivacaine + 10-kDa HA (Weight ratio 1:2)	Bupi HA (10-kDa) MN
4	Lidocaine + 300-kDa HA (Weight ratio 4:5)	Lido HA (300-kDa) MN

Visualization of microneedles

The surface morphology of the fabricated microneedles was visualized using scanning electron microscopy (SEM) (JEOL JSM-7500F, Japan) with an operation voltage of 15 kV. The microneedle patches were fixed on SEM stub and coated with a thin layer of carbon for the visualization. The microneedles containing rhodamine B were visualized by confocal laser scanning microscopy (ZEISS CLSM, Overkochen, Germany) by scanning them with a depth resolution of 5 μm/step using a 4× Plan Apo objective with a 4× magnification.

Micromanipulation

The detailed working principles of the micromanipulation technique have been introduced in previous studies [18,21]. Briefly, to start the compression, the microneedle patches were placed on the stage of the micromanipulation instrument equipped with a force transducer (Model GSO-10, Transducer Techniques, LLC, USA). An optical glass rod made of Borosilicate with a flat end of a diameter of 100 μm

was mounted onto the force transducer for the compression. Single microneedles were compressed between the stage and the glass probe with a compression speed of 2 μm/s. The applied force on single microneedles as a function of their displacement was recorded. One typical example of different status of the single microneedles during compression is shown in Figure 1. The compression process is shown in supplementary video. For each type of microneedles, 30 needles were measured.

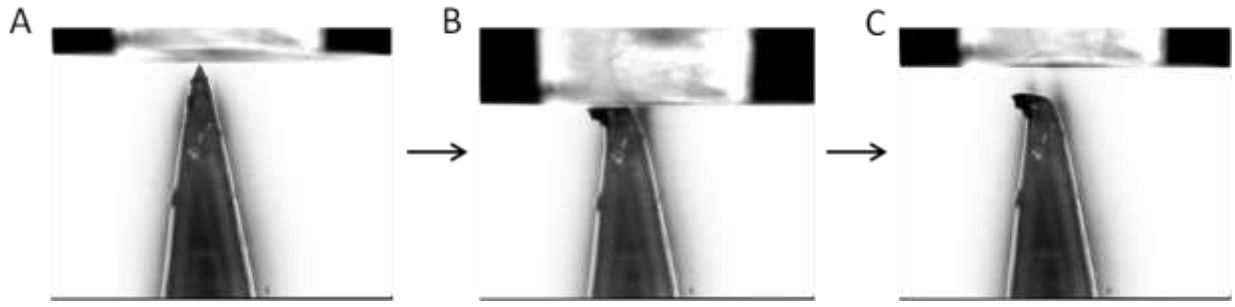

Figure 1. One example of different status of individual microneedle during the compression measurement. A: Before compression, B: Fracture of microneedles, C: After compression.

Calculation of the normal stress from compression force

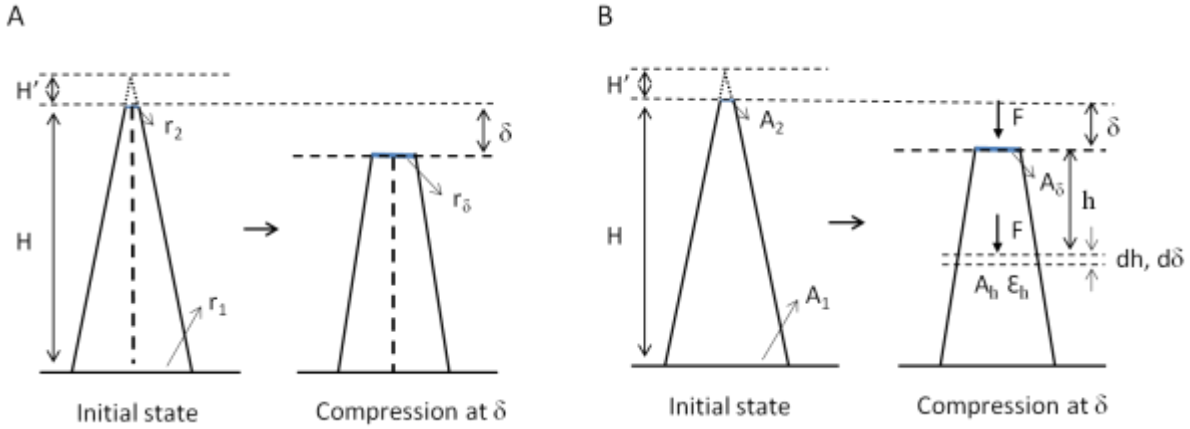

Figure 2. Schematic diagram for modeling of stress (A) and Young's modulus (B). Abbreviations: H: initial height of a microneedle. H': height of the missing tip when assuming the microneedle is perfectly sharp. r_1: half side length of a quadrangular microneedle base. r_2: initial half side length of the quadrangular microneedle tip. δ: displacement of the microneedle. r_δ: half side length of contact surface at a compressing displacement of δ. A_1: surface area of the quadrangular microneedle base. A_2: surface area of the quadrangular microneedle tip. A_δ: contact surface area at a compressing displacement of δ. F: compression force at a displacement of δ. h: height of the microneedle (from top of the microneedle) until sectional area of A_h. ε_h: deformation at a height of h. dh: the length of the element at h. dδ: displacement at h.

The normal stress was calculated from compression force using modeling as shown in Figure 2A. In this modeling, we ignored the volume change of microneedle and the deformation of microneedle base during compression (Figure 2A).

The volume of a single microneedle can be calculated by using dimension parameters as below (Eq.1).

$$V=4/3r_1^2(H+H')-4/3r_2^2H' \quad \text{(Eq.1)}$$

where V is the volume of the microneedle, r_1 is half side length of the quadrangular microneedle base, H is initial height of the microneedle, H' is height of the missing tip when assuming the microneedle is perfectly sharp and r_2 is half initial side length of the quadrangular microneedle tip.

According to geometric similarity (Eq.2)

$$H'/r_2=(H+H')/r_1 \quad \text{(Eq.2)}$$

By combining microneedle volume (Eq.1) and geometric similarity (Eq.2) equations, we can eliminate H' from the equations, and r_2 can be calculated from parameters which are already known (Eq.3).

$$r_2 = 1/2(-r_1 + \sqrt{3V/H - 3r_1^2}) \quad \text{(Eq.3)}$$

After replacing r_2 with r_δ and replacing H by H- δ at a compression displacement of δ, r_δ can be obtained (Eq.4).

$$r_\delta = 1/2(-r_1 + \sqrt{3V/(H-\delta) - 3r_1^2}) \quad \text{(Eq.4)}$$

Finally, the normal stress can be calculated by dividing compression force by the contacting area 4 r_δ^2 (Eq. 5).

$$\text{Normal stress} = F/(4r_\delta^2) \quad \text{(Eq.5)}$$

Young's modulus calculation

Young's modulus was calculated from compression force using a modeling as shown in Figure 2B.

We assumed that the microneedle was linearly elastic under a small deformation and only considered the longitudinal deformation. At a height of h (from the top of the microneedle) with the sectional area A_h, the deformation ε_h can be calculated by the stress-strain equation (Eq.6).

$$\varepsilon_h = \frac{F}{EA_h} \quad \text{(Eq. 6)}$$

Where F is the compression force, E is Young's modulus.

ε_h can also be given by

$$\varepsilon_h = \frac{d\delta}{dh} \quad \text{(Eq.7)}$$

where dδ is the displacement at h and dh is the length of the element at h.

From geometric similarity

$$\frac{A_h}{A_1} = \left(\frac{h + H'}{H + H'}\right)^2 \quad \text{(Eq. 8)}$$

Thus,

$$A_h = \left(\frac{h + H'}{H + H'}\right)^2 A_1 \quad \text{(Eq.9)}$$

The overall displacement δ can be calculated by integrating $d\delta$ over the microneedle as

$$\delta = \int_0^H d\delta \quad \text{(Eq.10)}$$

Submitting Eq.6 to 9 into Eq.10 leads to

$$\delta = \frac{F}{A_1 E}\int_0^H \frac{1}{\left(\frac{h + H'}{H + H'}\right)^2} dh \quad \text{(Eq.11)}$$

which can be written as follows

$$E = \frac{F}{\delta}\frac{(H+H')H}{A_1 H'} \quad \text{(Eq.12)}$$

Statistical analysis

In total 30 microneedles from each type of samples were analyzed. All the data of the mechanical properties were analyzed by one way ANOVA with Turkey's post-test using GraphPad Prism software (version 5.02). The significance levels were set at *p<0.05, **p<0.01, and ***p<0.001.

3. Results

Morphology of microneedles

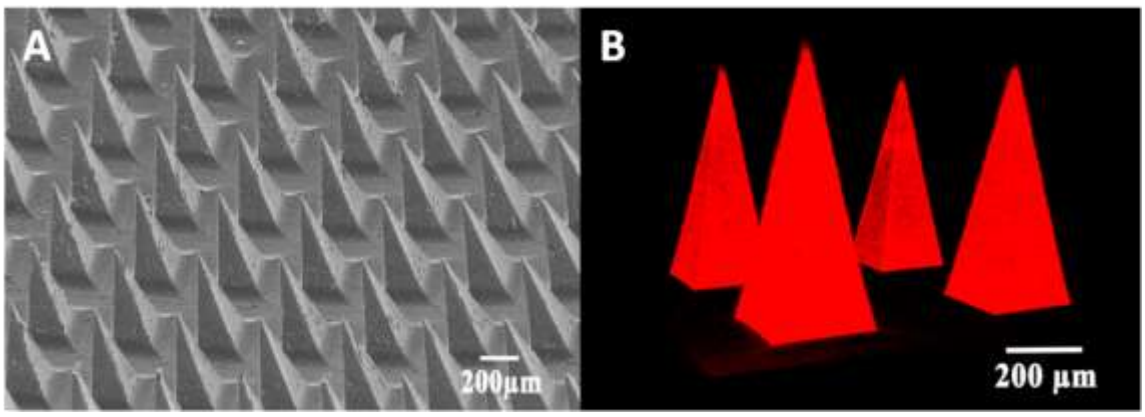

Figure 3. Representative microscopy images of the fabricated microneedles. A: Scanning electronic microscopy (SEM) images. B: Confocal laser scanning microscopy (CLSM) images.

The microscopy images of representative microneedles in a patch are shown in Figure 3. SEM (Figure 3A) and CLSM (Figure 3B) images show that the obtained microneedles had a regular quadrangular pyramid shape and sharp tips.

Force versus displacement and normal stress versus displacement curves

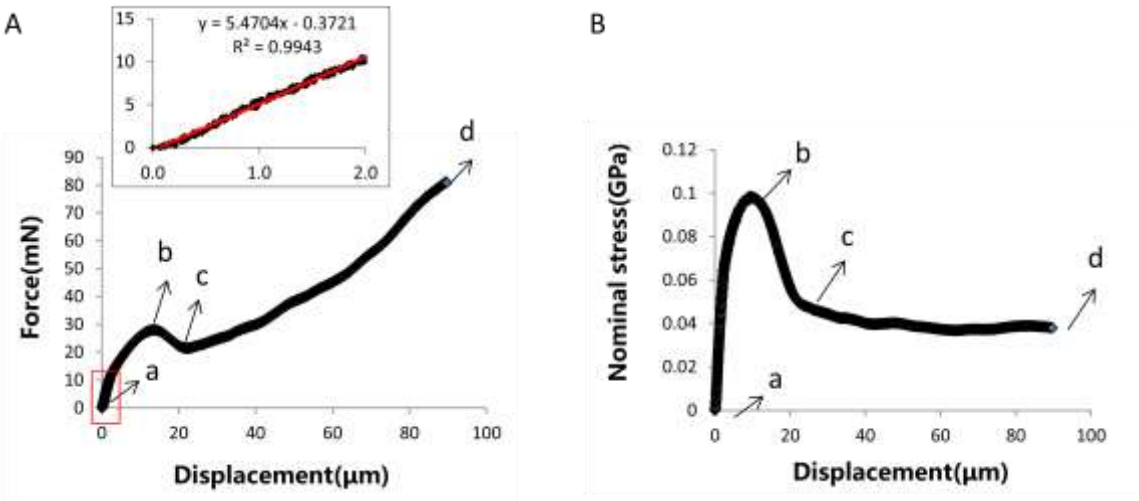

Figure 4. Typical force versus displacement (A) and the corresponding normal stress versus displacement (B) curves obtained from compression of a single microneedle.

A typical relationship of the force applied on an individual microneedle and the corresponding normal stress as a function of the probe moving distance (displacement) is shown in Figure 4A and 4B, respectively. Immediately after point-a the probe touched the microneedle tip, the force increased until point-b at which the microneedle ruptured (Figure 4A). As a result, the force decreased to point-c and increased again until reaching the detection limitation of the sensor at point-d. Figure 4B shows the derived normal stress-displacement curve. In contrast, the normal stress increased from point-a to peak point-b when the needle ruptured, after which the stress decreased to point-c and reached a plateau where it stayed roughly the same until the end of the measurement (point-d). From these curves, the rupture force and rupture stress (normal stress at rupture) can be determined (point-b). The rupture displacement is identified as the distance that the probe travels from point-a until point-b when the microneedle ruptures. The video of the compression process is shown in Supplementary information.

Summary of the rupture displacements

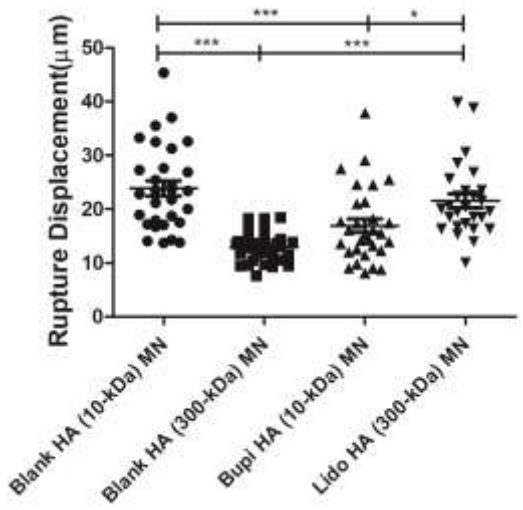

Figure 5. Rupture displacements of various types of microneedles. *:p<0.05; **:p<0.01;***:p<0.001.

We summarized the rupture displacements of different types of microneedles in Figure 5. It is shown that Blank HA (300-kDa) MN patch had the narrowest distribution of rupture displacement among all patches. Specifically, the characterized patches showed an average rupture displacement between 12.9 ± 2.8 μm (Blank HA (300-kDa) MN) and 23.8 ± 7.9 μm (Blank HA (10-kDa) MN). The rupture displacement of microneedles made of 10-kDa HA (23.8 ± 7.9 μm) was significantly higher than that of microneedles made of 300-kDa HA (12.9 ± 2.8 μm). The drug loaded patch showed either a lower (Bupi HA (10-kDa) MN, 16.9 ± 6.9 μm) or higher (Lido HA (300-kDa) MN, 21.6 ±6.8 μm) rupture displacement than the corresponding blank HA patches.

Summary of rupture forces and stresses

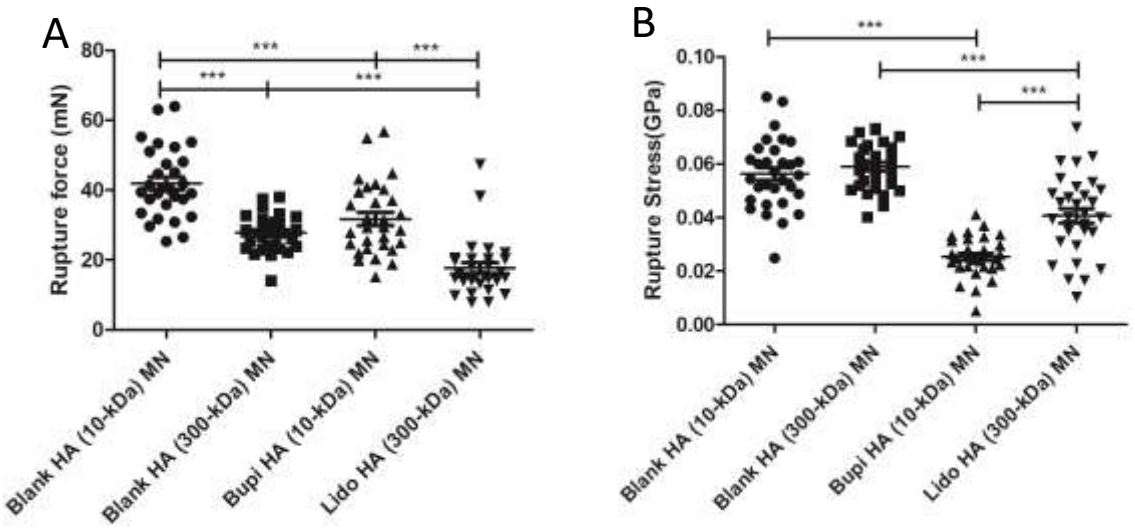

Figure 6. Rupture forces and stresses of different types of microneedles. *:p<0.05; **:p<0.01;***:p<0.001.

The rupture forces and stresses of different types of microneedle patches are summarized and presented in Figure 6. In case of rupture force, blank microneedles made of 10-kDa HA showed a mean rupture force of 42.0 ± 9.9 mN, which was significantly higher than that of the microneedles made of 300-kDa HA (27.7 ± 5.2 mN). The loading of drug in HA (10-kDa) MN and HA (300-kDa) MN significantly decreased the rupture force of the corresponding microneedles to 31.7 ± 10.3 mN and 17.7 ± 8.3 mN, respectively. As for rupture stress, by contrast, blank microneedles made of 10-kDa and 300-kDa HA showed similar rupture stresses of 0.072 ± 0.017 GPa and 0.075 ± 0.011 GPa. The loading of drug into the microneedles made of 10-kDa and 300-kDa HA significantly decreased the rupture stresses by around 50% and 25%, respectively.

Young's modulus of the microneedles

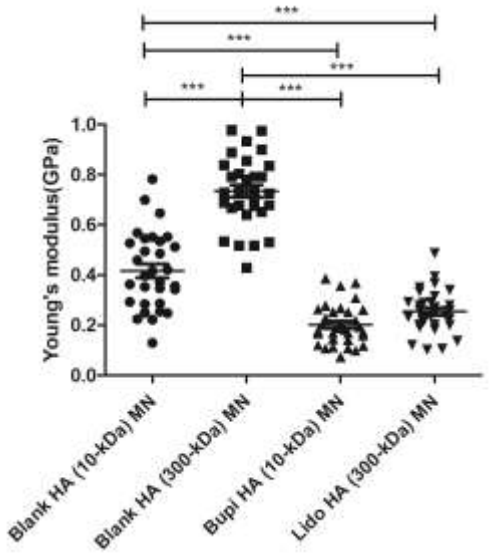

Figure 7. Calculated Young's modulus of different types of microneedles. *:p<0.05; **:p<0.01;***:p<0.001

The relationship between force and displacement was found be linear for displacements up to 2 µm, as predicted by the elastic model (Eq.9), which was used to calculate the Young's modulus of different microneedles via liner regression (see insert of Figure 4A) and the Young's modulus values are presented in Figure 7. Interestingly, blank microneedles made of 300-kDa HA showed a significantly higher Young's modulus than that made of 10-kDa HA. The incorporation of drugs into microneedles also significantly decreased the Young's modulus of the microneedles: the loading of bupivacaine into 10-kDa HA MN slightly decreased the Young's modulus from 0.42 ± 0.15 to 0.20 ± 0.08 GPa while the loading of lidocaine into 300-kDa HA microneedles robustly decreased the Young's modulus from 0.73 ± 0.14 to 0.25 ± 0.09 GPa.

4. Discussion and conclusions

One aim of this study was to investigate the potential of the micromanipulation technique for characterization of the mechanical properties of polymeric microneedles. We therefore fabricated HA microneedles with two different molecular weights with or without loaded model drugs. We measured

and compared their mechanical properties with micromanipulation. Our results showed that the micro-manipulation technique is a powerful tool for precise and comprehensive characterization of the mechanical properties of polymeric microneedles. The change of the compression force as a function of displacement behavior of single microneedles can be precisely recorded during the compression. With this information as well as mathematic modeling, the normal stress at the contact area between the force probe and the microneedle as a function of its displacement and several important mechanical/material property parameters including displacement at rupture, rupture force and Young's modulus can be analyzed and calculated. As compared to bulk compression strategies, micromanipulation has at least two advantages. Firstly, in comparison with different bulk compression strategies as previously reported, which assume all microneedles within one patch have the same mechanical strength, micro-manipulation can directly and precisely measure the rupture behavior of individual microneedles, therefore can give information on the uniformity of the microneedle strength across the patch. Our data indeed showed that the mechanical property parameters of microneedles across one patch can vary significantly (Figure 5-7). Secondly, the bulk compression strategies only measure rupture forces to evaluate the mechanical property of microneedle patches. Additionally, we compressed the whole patch of Blank HA (10-KDa) MN with a traditional strategy. We even could not observe a clear rupture behavior of the patch (Supplementary Figure 1). In micro-manipulation, as shown in our results, other parameters including displacement at rupture, rupture stress as well as intrinsic material properties such as Young's modulus can also be measured. Therefore, the micromanipulation technique can be used to comprehensively evaluate the mechanical properties of microneedles within one patch and to compare the difference in mechanical properties among different type of patches.

During the measurement, we obtained in total four mechanical/material property parameters that can reflect the mechanical strength of microneedles, including displacement at rupture, rupture force, rupture stress and Young's modulus. Young's modulus can reflect the stiffness of the measured sample, while displacement at rupture describes the maximum deformation level before the rupture of microneedles [25,26]. Both of these two indicators can be used for comparison of the mechanical strength of different microneedles when the measured microneedles are made of the same materials. This is indicated by our results that although Blank HA (10-kDa) MN showed a lower Young's modulus (Figure 7), they showed a higher rupture force as compared to the Blank HA (300-kDa) MN (Figure 6). On the other hand, Blank HA (10-kDa) MN showed a much higher rupture displacement than Blank HA (300-kDa) MN (Figure 5), but they own a similar rupture stress to the later one (Figure 6).

Most of the reported studies made use of rupture force of the microneedles for evaluation of the mechanical strength of microneedles [8,10,27,28]. However, our results showed that rupture force and rupture stress results could give different trends. For example, based on rupture force results, Blank HA (10-kDa) MN is mechanically stronger than Blank HA (300-kDa) MN (Figure 6A). However, their mechanical strengths are similar according to rupture stress results (Figure 6B). Actually, the rupture force of microneedles could be significantly affected by the rupture displacement/contacting area at rupture. As a result, simple comparison of rupture force is not enough for the evaluation of the mechanical strength of different microneedle patches since it is not an intrinsic material property

parameter. In contrast, the rupture stress of microneedles can be considered to be an intrinsic material parameter, and our results indicated that it is a better indicator for the mechanical strength of polymer microneedles as compared to rupture force. The rupture stress results in the current study indicated that among the different type of microneedles that were investigated, Blank HA (10-kDa) MN and Blank HA (300-kDa) MN have a similar mechanical strength, but are all stronger than their corresponding drug loaded microneedle patches.

Our results in this study showed that both the molecular weight of the polymer and the loading of drug could significantly influence the mechanical properties of microneedles. We showed that blank microneedles made of 300-kDa HA had a significantly higher Young's modulus than that made of 10-kDa HA. This observed trend is consistent with a previous study showing that 50 kDa HA gel had a significantly higher elastic modulus than 10-kDa HA gel [29]. However, as discussed above, the greater Young's modulus of Blank HA (300-kDa) MN did not simply lead to a greater rupture stress because it was ruptured at smaller displacement/deformation. Sun et al. also [28] showed that the tensile strength of a material was proportional to Young's modulus for a given material, but the relationship can vary significantly with materials. On the other hand, our results showed that the loading of both lidocaine hydrochloride and bupivacaine hydrochloride significantly decreased the mechanical strength of the microneedles, as shown by the results of rupture force, rupture stress and Young's modulus of the microneedles (Figure 6-7). These results are consistent with previous reports. For instance, Park et al. [13] showed that the loading of calcein or bovine serum albumin into poly-lactide-co-glycolic (PLGA) based microneedles could significantly decrease the mechanical strength of the microneedles. These findings indicated that the mechanical strength of the microneedles was mainly contributed by the polymer matrix and the poor adhesion between the drug and polymer could cause mechanical failure sites for the microneedles [13]. Nevertheless, previous research has indicated that the ultimate rupture stress of skin was around 0.027 ± 0.009 GPa. Our measured rupture stress results of microneedle patches except Bupi HA (10-kDa) are higher than this value, indicating that these microneedles may be strong enough for piercing of the skin [30,31]. It should be noted that the environmental factors including temperature and air humidity could significantly affect the mechanical property of HA microneedles. For instance, Wang et al. has observed that after storing HA microneedles in 60% relative humidity for 30 min at 25 °C, the mechanical strength of the microneedles became significantly lower [32]. The environmental factors will be closely monitored in our future measurements.

In conclusion, our studies showed that the micromanipulation technique is an effective tool for precise characterization of the mechanical properties of polymeric microneedles. The generated information could provide important information for rational design of polymeric microneedles with sufficient mechanical strength for skin penetration. The results also revealed that we should carefully evaluate the variations among the microneedles across the patches and pay attention to the influence of drug loading and molecular weight of the polymer microneedles on their mechanical strength.

Acknowledgements

We acknowledge the financial support of the National Natural Science Foundation of China (No. 81961130395), China Postdoctoral Science Foundation Grant (2019M663534), Program of Introducing

Talents of Discipline to Universities (Plan 111, No. B18035), and NAF\R1\191217 - Newton Advanced Fellowships 2019.

Conflict of interest

There is no conflict of interest.

References:

1. Ye Y, Yu J, Wen D, Kahkoska AR, Gu Z: **Polymeric microneedles for transdermal protein delivery**. *Adv Drug Deliv Rev* 2018, **127**:106-118.
2. Wang M, Hu L, Xu C: **Recent advances in the design of polymeric microneedles for transdermal drug delivery and biosensing**. *Lab Chip* 2017, **17**:1373-1387.
3. Lee JW, Han MR, Park JH: **Polymer microneedles for transdermal drug delivery**. *Journal of Drug Targeting* 2013, **21**:211-223.
4. Kim YC, Park JH, Prausnitz MR: **Microneedles for drug and vaccine delivery**. *Adv Drug Deliv Rev* 2012, **64**:1547-1568.
5. Du G, Sun X: **Current Advances in Sustained Release Microneedles**. *Pharmaceutical Fronts* 2020, **02**:e11-e22.
6. Gittard SD, Chen B, Xu H, Ovsianikov A, Chichkov BN, Monteiro-Riviere NA, Narayan RJ: **The Effects of Geometry on Skin Penetration and Failure of Polymer Microneedles**. *J Adhes Sci Technol* 2013, **27**:227-243.
7. Park JH, Prausnitz MR: **Analysis of Mechanical Failure of Polymer Microneedles by Axial Force**. *J Korean Phys Soc* 2010, **56**:1223-1227.
8. Yu JC, Wang JQ, Zhang YQ, Chen GJ, Mao WW, Ye YQ, Kahkoska AR, Buse JB, Langer R, Gu Z: **Glucose-responsive insulin patch for the regulation of blood glucose in mice and minipigs**. *Nature Biomedical Engineering* 2020, **4**:499-506.
9. Yu JC, Zhang YQ, Kahkoska AR, Gu Z: **Bioresponsive transcutaneous patches**. *Current Opinion in Biotechnology* 2017, **48**:28-32.
10. Wang J, Ye Y, Yu J, Kahkoska AR, Zhang X, Wang C, Sun W, Corder RD, Chen Z, Khan SA, et al.: **Core-Shell Microneedle Gel for Self-Regulated Insulin Delivery**. *ACS Nano* 2018, **12**:2466-2473.
11. Yang PP, Lu C, Qin WB, Chen ML, Quan GL, Liu H, Wang LL, Bai XQ, Pan X, Wu CB: **Construction of a core-shell microneedle system to achieve targeted co-delivery of checkpoint inhibitors for melanoma immunotherapy**. *Acta Biomaterialia* 2020, **104**:147-157.
12. Donnelly RF, Singh TR, Garland MJ, Migalska K, Majithiya R, McCrudden CM, Kole PL, Mahmood TM, McCarthy HO, Woolfson AD: **Hydrogel-Forming Microneedle Arrays for Enhanced Transdermal Drug Delivery**. *Adv Funct Mater* 2012, **22**:4879-4890.
13. Park JH, Allen MG, Prausnitz MR: **Polymer microneedles for controlled-release drug delivery**. *Pharm Res* 2006, **23**:1008-1019.
14. van der Maaden K, Sekerdag E, Jiskoot W, Bouwstra J: **Impact-insertion applicator improves reliability of skin penetration by solid microneedle arrays**. *AAPS J* 2014, **16**:681-684.
15. Vallhov H, Xia W, Engqvist H, Scheynius A: **Bioceramic microneedle arrays are able to deliver OVA to dendritic cells in human skin**. *Journal of Materials Chemistry B* 2018, **6**:6808-6816.
16. Dardano P, Caliò A, Palma VD, Bevilacqua MF, Matteo AD, Stefano LD: **A Photolithographic Approach to Polymeric Microneedles Array Fabrication**. *Materials* 2015, **8**.
17. Nguyen-Tri P, Ghassemi P, Carriere P, Nanda S, Nguyen DD: **Recent Applications of Advanced Atomic Force Microscopy in Polymer Science: A Review**. *Polymers* 2020, **12**:1142.

18. Zhang Z, Ferenczi MA, Lush AC, Thomas CR: **A novel micromanipulation technique for measuring the bursting strength of single mammalian cells**. *Appl Microbiol Biotechnol* 1991, **36**:208-210.
19. Gray A, Egan S, Bakalis S, Zhang ZB: **Determination of microcapsule physicochemical, structural, and mechanical properties**. *Particuology* 2016, **24**:32-43.
20. Olderoy MO, Xie ML, Andreassen JP, Strand BL, Zhang ZB, Sikorski P: **Viscoelastic properties of mineralized alginate hydrogel beads**. *Journal of Materials Science-Materials in Medicine* 2012, **23**:1619-1627.
21. Long Y, Song K, York D, Zhang Z, Preece JA: **Engineering the mechanical and physical properties of organic–inorganic composite microcapsules**. *Colloids and Surfaces A: Physicochemical and Engineering Aspects* 2013, **433**:30-36.
22. Nguyen BV, Wang QG, Kuiper NJ, El Haj AJ, Thomas CR, Zhang ZB: **Biomechanical properties of single chondrocytes and chondrons determined by micromanipulation and finite-element modelling**. *Journal of the Royal Society Interface* 2010, **7**:1723-1733.
23. Zhang ZB, Sisk ML, Mashmoushy H, Thomas CR: **Characterisation of the breaking force of latex particle aggregates by micromanipulation**. *Particle & Particle Systems Characterization* 1999, **16**:278-283.
24. Monkare J, Pontier M, van Kampen EEM, Du GS, Leone M, Romeijn S, Nejadnik MR, O'Mahony C, Slutter B, Jiskoot W, et al.: **Development of PLGA nanoparticle loaded dissolving microneedles and comparison with hollow microneedles in intradermal vaccine delivery**. *European Journal of Pharmaceutics and Biopharmaceutics* 2018, **129**:111-121.
25. Hu JF, Chen HQ, Zhang ZB: **Mechanical properties of melamine formaldehyde microcapsules for self-healing materials**. *Materials Chemistry and Physics* 2009, **118**:63-70.
26. Stubna I, Trnik A, Sin P, Sokolar R, Medved' I: **Relationship between Mechanical Strength and Young's Modulus in Traditional Ceramics**. *Materiali in Tehnologije* 2011, **45**:375-378.
27. Sullivan SP, Murthy N, Prausnitz MR: **Minimally invasive protein delivery with rapidly dissolving polymer microneedles**. *Advanced Materials* 2008, **20**:933-+.
28. Pan J, Ruan W, Qin M, Long Y, Wan T, Yu K, Zhai Y, Wu C, Xu Y: **Intradermal delivery of STAT3 siRNA to treat melanoma via dissolving microneedles**. *Sci Rep* 2018, **8**:1117.
29. Kim J, Park Y, Tae G, Lee KB, Hwang CM, Hwang SJ, Kim IS, Noh I, Sun K: **Characterization of low-molecular-weight hyaluronic acid-based hydrogel and differential stem cell responses in the hydrogel microenvironments**. *Journal of Biomedical Materials Research Part A* 2009, **88A**:967-975.
30. Groves RB, Coulman SA, Birchall JC, Evans SL: **Quantifying the mechanical properties of human skin to optimise future microneedle device design**. *Comput Methods Biomech Biomed Engin* 2012, **15**:73-82.
31. Gallagher AJ, Annaidh AN, Bruyère K, et al.: **Dynamic Tensile Properties of Human Skin**. International Research Council on the Biomechanics of Injury; 2012.
32. Wang QL, Ren JW, Chen BZ, Jin X, Zhang CY, Guo XD: **Effect of humidity on mechanical properties of dissolving microneedles for transdermal drug delivery**. *Journal of Industrial and Engineering Chemistry* 2018, **59**:251-258.